


A model framework to investigate the role of anomalous land surface processes in the amplification of summer drought across Ireland during 2018

Kazeem A. Ishola^{1,2}  | Gerald Mills³ | Reamonn M. Fealy² | Rowan Fealy¹

¹Irish Climate Analysis and Research Units (ICARUS), Department of Geography, Maynooth University, Maynooth, Ireland

²Teagasc Agrifood Business and Spatial Analysis Department, Ashtown, Ireland

³School of Geography, University College Dublin, Dublin, Ireland

Correspondence

Kazeem A. Ishola, Irish Climate Analysis and Research Units (ICARUS), Department of Geography, Maynooth University, Maynooth, Ireland.
Email: kazeem.ishola.2018@mumail.ie

Funding information

Teagasc-the Agriculture and Food Development Authority, Grant/Award Number: 2016076

Abstract

Due to its latitude and ample year-round rainfall, Ireland is typically an energy-limited regime in the context of soil moisture availability and evapotranspiration. However, during the summer of 2018, regions within the country displayed significant soil moisture deficits, associated with anomalous atmospheric forcing conditions, with consequent impacts on the surface energy balance. Here, we explore the utility of a physically based land surface scheme coupled with observational, global gridded reanalysis and satellite-derived data products to analyse the spatial and temporal evolution of the 2018 summer drought event in Ireland over grassland, which represents the dominant agricultural land-cover. While the surface–air energy exchanges were initially dominated by atmospheric anomalies, soil moisture constraints became increasingly important in regulating these exchanges, as the accumulated rainfall deficit increased throughout the summer months. This was particularly evident over the freer draining soils in the east and southeast of the country. From late June 2018, we identify a strong linear coupling between soil moisture and both evapotranspiration and vegetation response, suggesting a shift from an energy-limited evapotranspiration regime into a dry or soil water-limited regime. Applying segmented regression models, the study quantifies a critical soil moisture threshold as a key determinant of the transition from wet to dry evaporative regimes. These findings are important to understand the soil moisture context under which land–atmosphere couplings are strongest in water-limited regimes across the country and should help improve the treatment of soil parameters in weather prediction models, required for subseasonal and seasonal forecasts, consequently enhancing early warning systems of summer climate extremes in the future.

KEYWORDS

climate extremes, drought, evaporative fraction, land–atmosphere interactions, soil moisture, surface energy budget

This is an open access article under the terms of the [Creative Commons Attribution](https://creativecommons.org/licenses/by/4.0/) License, which permits use, distribution and reproduction in any medium, provided the original work is properly cited.

© 2022 The Authors. *International Journal of Climatology* published by John Wiley & Sons Ltd on behalf of Royal Meteorological Society.

1 | INTRODUCTION

During the past two decades, regions across Europe have experienced hot summers and drought events, which varied in terms of the development, frequency, intensity and impacts (e.g., Buras *et al.*, 2019). Droughts are typically categorized as either meteorological (high rainfall deficits), hydrological (extremely low groundwater, lakes, streamflow, etc.), agricultural (high soil moisture deficits, affecting vegetation) or socioeconomic, when the demand for water exceeds the supply (van Loon, 2015; Falzoi *et al.*, 2019). A meteorological drought precedes agricultural drought through reduction in soil water storage and the water available for uptake by roots (Buitink *et al.*, 2020), but to fully understand the development of these events, other factors such as changes to soil and biophysical properties must be taken into account. While there have been many studies on agricultural droughts across Europe (e.g., Noone *et al.*, 2017; Falzoi *et al.*, 2019; Buitink *et al.*, 2020; van Hateren *et al.*, 2021), there have been few investigations in Ireland, where such events are rare.

The 2018 European summer (April–August) was associated with a higher near-surface temperature and lower rainfall receipts relative to the long-term (1981–2010) mean (Magnusson *et al.*, 2018). These conditions were created by a large and persistent anticyclonic system located over central and northern Europe, which blocked the normal passage of Atlantic storms (Buras *et al.*, 2019; Kornhuber *et al.*, 2019; Rösner *et al.*, 2019; Dirmeyer *et al.*, 2021). The resulting heatwave and drought were extreme, surpassing previous records with several stations across Europe reporting record breaking daily maximum temperatures (Buras *et al.*, 2019; Rösner *et al.*, 2019; Dirmeyer *et al.*, 2021). Ireland, situated on the western maritime fringe of Europe, experienced unusually warm and dry conditions (Moore, 2020) that impacted on grass growth productivity and farm income (Dillon *et al.*, 2018). These impacts were preconditioned by the cold ground temperature arising from the exceptional snow fall that was associated with cold air mass advecting around high pressure from Siberia towards the country dubbed the “Beast from the East,” from the end of February and lasted for about a week, resulting in a late onset of grass growth, by about a month relative to an average year (Dillon *et al.*, 2018).

When drought and heatwave events evolve simultaneously, they can reinforce each other. The occurrence of these “compound” events and the associated land–air exchanges have been observed across Europe over the last few decades (e.g., 2003, 2010, 2015, 2018). For instance, Black *et al.* (2004) demonstrated that the events of August 2003 across Europe were exacerbated by the

persistence of the anticyclonic blockage that enhanced the net radiative flux and reduced water availability, such that the surface–air sensible heat flux was increased leading to elevated air temperatures (i.e., a positive feedback) and increased atmospheric water demand. Compound events can result in a wide range of impacts including water scarcity, tree mortality, agricultural loss, wildfires and air pollution with deleterious effects on ecosystems, human health and well-being and agricultural productivity (Fink *et al.*, 2004; Conti *et al.*, 2005; García-Herrera *et al.*, 2010; Alexander, 2011; Dole *et al.*, 2011; Zscheischler *et al.*, 2018; Miralles *et al.*, 2019; Schuldt *et al.*, 2020).

The transition from meteorological to agricultural drought is closely linked to the plant available soil moisture (θ) during the growing season. Broadly speaking, evapotranspiration (ET) can be categorized into energy- and water-limited regimes. In the latter, increasing soil moisture deficits and atmospheric evaporative demand causes vegetation to close stomata to limit water loss to the atmosphere; the associated decrease in the latent heat flux with surplus energy being channelled into sensible heat initiates the positive feedback with near surface air temperature described above (Seneviratne *et al.*, 2010; Miralles *et al.*, 2019). The transition from energy- to water-limited regimes occurs at a critical soil moisture (θ_c) value and landscapes can switch between regimes over the course of a year depending on precipitation, available surface energy, atmospheric demand and the status of vegetative cover (Knist *et al.*, 2017).

The evaporative fraction (EF), defined as the ratio of latent heat flux and available energy at the land surface and can be expressed as a function of θ (Seneviratne *et al.*, 2010; Buitink *et al.*, 2020; Denissen *et al.*, 2021), has previously been used to evaluate vegetative productivity. Buitink *et al.* (2020) used a similar framework but replaced the EF with satellite-derived ecosystem indicators, near infrared reflectance of vegetation (NIRv) and vegetation optical depth (VOD), to allow for a more precise analysis of how productivity was related to θ during the 2018 drought event at two sites in the Netherlands. A number of other studies have derived values for θ_c based on observations and model outputs using alternative theoretical frameworks (Akbar *et al.*, 2018; Haghghi *et al.*, 2018; Feldman *et al.*, 2019; Denissen *et al.*, 2020). Determining θ_c is critical for predicting the timescales of plant responses, ET decay and consequently the emergence and progression of agricultural drought.

This research uses a simple land surface scheme, which employs readily available meteorological and surface data, to investigate the role of land–atmosphere exchange processes across Ireland during the 2018 summer drought. The study seeks to analyse (a) the evolution of the 2018 drought at sub seasonal and regional

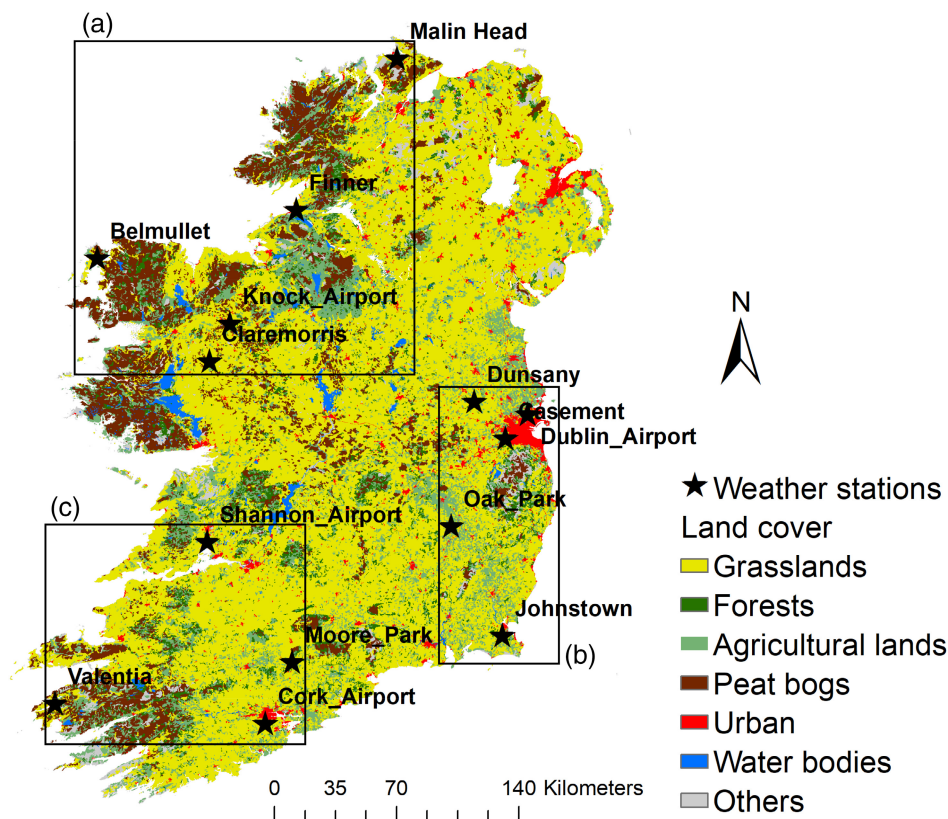


FIGURE 1 Map of the study area showing the locations of selected weather stations and the dominant land cover types from 2018 CORINE Land cover product. The boxes A, B and C comprise of the stations grouped on the basis of similar precipitation regimes and agricultural regions [Colour figure can be viewed at [wileyonlinelibrary.com](https://onlinelibrary.wiley.com/doi/10.1002/joc.7785)]

scales; (b) the anomalies in simulated land–atmosphere energy exchanges; and (c) the role of soil moisture in modulating land–atmosphere exchange processes. We combine a physically based land surface scheme with observational data, along with readily accessible global ERA5-Land gridded reanalysis and satellite-derived data products to address these objectives. The scheme used here has previously been established as having the capability to reproduce measured surface fluxes (de Rooy and Holtslag, 1999; Ishola *et al.*, 2020). The method outlined offers the potential for improving management strategies, particularly during anomalous warm and dry events, and for delineating areas with differential drought responses.

While the global ERA5-Land model provides estimates of land fluxes, these fluxes may not adequately capture the dynamic process at the point/field scale of the current study due to the model grid (9 km²) and/or the microscale variations in land surface. Additionally, the skill of ERA5-Land in replicating the land fluxes over Ireland is broadly unknown. In contrast, the LSS employed here has previously been evaluated for selected sites in Ireland. Importantly, and a core motivation for the study is that the LSS employed allows to control, and adjust, model parameters in order to explore relationships with the aim of improving model representation.

2 | MATERIALS AND METHODS

2.1 | Study area

The Island of Ireland (Figure 1) has a maritime temperate climate (Peel *et al.*, 2007) with a long-term (1981–2010) mean daily maximum temperature of between 18 and 20°C in summer. In winter, daily minimum temperatures occasionally drop below 0°C, but average winter temperatures are generally around 8°C. Ireland receives an annual average rainfall of over 1,200 mm, distributed throughout the year. The spatial distribution of rainfall follows a west to east gradient; higher rainfall receipts (~1,000–1,400 mm) typically occur on the west coast and particularly in the upland regions where receipts can exceed 2,000 mm largely associated with topographic interactions with the prevailing maritime air. Lower rainfall amounts are experienced in the east of the country (~750–1,000 mm) (Met Éireann). A summary description of the climatology of the region is reported in Walsh (2012).

The most important biome in Ireland is that of grassland, which accounts for 56% of the total land area (McEniry *et al.*, 2013) and more than 90% of agricultural land cover (Figure 1). Due to the favourable growing conditions, grass growth can occur throughout the year, particularly along the coastal margins in the south of the

TABLE 1 Characteristics of the selected grassland synoptic stations

Station	Lat/lon (°N, °W)	Elevation (m)	Soil type	Drainage class	Region	Zone
Belmullet	54.228, 10.007	9	Peat	Poor	Northwest	
Claremorris	53.711, 8.991	69	Coarse loam	Well	Northwest	
Finner	54.494, 8.243	33	Coarse loam	Poor	North	A
Knock Airport	53.906, 8.817	201	Fine loam	Imperfect	Northwest	
Malin Head	55.372, 7.339	20	Peat	Poor	North	
Casement	53.306, 6.439	91	Fine loam	Moderate	East	
Dublin Airport	53.428, 6.241	71	Fine loam	Moderate	East	
Dunsany	53.499, 6.699	83	Fine loam	Moderate	East	B
Johnstown Castle	52.292, 6.489	52	Fine loam	Imperfect	Southeast	
Oak Park	52.861, 6.915	62	Fine loam	Moderate	Southeast	
Cork Airport	51.847, 8.486	155	Fine loam	Well	South	
Moorepark	52.164, 8.264	46	Coarse loam	Well	South	
Shannon Airport	52.689, 8.918	15	Loam	Well	Southwest	C
Valentia	51.929, 10.239	24	Coarse loam	Well	Southwest	

Note: The soil types and drainage categories are based on the data from Irish Soil Information System (Creamer *et al.*, 2014). The grouped zones, A, B and C, comprise of stations with similar precipitation regimes.

country. The low cost of grass production here offers a significant competitive advantage to farmers and positively impacts on the low economic margins associated with agricultural production. However, grass growth is more problematic in the wet soils in the west and north of the country due to the heavier (clayey) soils (Keane and Collins, 2004), compared to the more freely draining soils that characterize the east and southeast region (Creamer *et al.*, 2014; McDonnell *et al.*, 2018). Detailed soil properties and information for Ireland is available from Creamer *et al.* (2014).

2.2 | Observational data

Hourly meteorological observations were obtained from 14 automatic weather stations (AWS) across Ireland (Table 1 and Figure 1) from the Irish national meteorological service, Met Éireann. These stations are sited over short grass cover, consistent with World Meteorological Organisation (WMO) guidelines, and report on global solar radiation ($Q_{s\downarrow}$, $W\cdot m^{-2}$) or sun duration (hr), air temperature ($^{\circ}C$), relative humidity (%), pressure (kPa), wind speed ($m\cdot s^{-1}$) and precipitation (mm). Cloud amount is required as an input but, as the observations are only available at relatively few stations, we subsequently exclude the cloud input in the land surface scheme to ensure consistency in approach across all stations. For stations where only sunshine hours are available, including Knock Airport, Casement (Aerodrome),

Shannon Airport and Cork Airport, hourly $Q_{s\downarrow}$ data were estimated for these stations based on observations of sunshine duration following Allen *et al.* (1998) and Ishola *et al.* (2018). The hourly meteorological observations were obtained for the summer months of May to August—the period over which the 2018 drought began and subsequently intensified. Due to the differences in the start of operations of a number of the AWS, we focus the main analysis on the most recent decade (2010–2019) to ensure consistent temporal coverage of meteorological data across all stations.

2.3 | Gridded meteorological data

Gridded daily total precipitation data for Ireland was also obtained from Met Éireann for the period from 1999 to 2019. This data, available at $1\ km^2$ grid resolution, was generated using interpolation techniques applied to in situ rainfall data from over 500 rainfall stations distributed across Ireland (Walsh, 2012).

The land surface scheme (LSS) employed here requires soil moisture measurements but these are not part of routine observational practice in Ireland, as in many other countries, and therefore we employed gridded reanalysis soil moisture data from the European Centre for Medium Range Weather Forecasting (ECMWF) ERA5-Land data, obtained from the C3S Copernicus Climate Data Store. ERA5-Land is the latest global reanalysis product from ECMWF, which employs

improved historical observations and is run at a finer spatial resolution (atmosphere 0.25° ; land 0.1°) relative to its predecessor, ERA-Interim (Hersbach and Dee, 2016). This product has also been evaluated at the global scale (e.g., Li *et al.*, 2020). We used ERA5-Land hourly volumetric water content (θ) ($\text{m}^3\cdot\text{m}^{-3}$) in the top soil layer (0–7 cm), for the period 1999–2019.

2.4 | Satellite-derived data products

The leaf area index (LAI) quantifies the greenness of plants and can be observed per unit horizontal surface area from space. LAI was obtained from the Copernicus Global Land Service (CGLS), which is derived from SPOT-VGT and PROBA-V, prior to and from 2014, respectively. The CGLS LAI product, beginning in 1999, employed SPOT-VGT; the method by Baret *et al.* (2013) has been used to retrieve LAI from PROBA-V. Here, we use the CGLS LAI GEOV2 product which is at 1 km^2 spatial and 10-day temporal resolution (Albergel *et al.*, 2019), to broadly assess the spatial representation and extent of the impact of 2018 drought on vegetation state across Ireland. The product development is outlined by Verger *et al.* (2014).

The land surface temperature (T_s) is a critical parameter that governs the land-atmosphere coupling and can be used to evaluate model derived estimates of surface energy fluxes. We acquired T_s from the Moderate Resolution Imaging Spectroradiometer (MODIS) (MOD11A1, version 6) from the Land Processes Distributed Active Archive Center (LP DAAC) (Wan *et al.*, 2015). In addition, the near-infrared radiation reflected by vegetation (NIRv) is an important index for monitoring ecosystem functioning and has previously been employed to link soil moisture induced vegetation stress with gross primary productivity (GPP) at various scales during drought events (Badgley *et al.*, 2017; 2019; Baldocchi *et al.*, 2020; Buitink *et al.*, 2020). The NIRv index is derived from the product of the normalized difference vegetation index (NDVI) and near infra-red (NIR) reflectance ($\text{NIRv} = \text{NDVI} \times \text{NIR}$) (e.g., Badgley *et al.*, 2017). We obtained daily MODIS (MCD43A4, version 6) red (620–670 nm) and NIR (841–876 nm) nadir-adjusted reflectance images from the same source (Schaaf and Wang, 2015). The MODIS T_s and reflectance images are available at 1 km^2 and 500 m^2 resolutions, respectively and were obtained for the period of 2010–2019 to correspond with the period of AWS measurements outlined in section 2.2. The T_s data obtained was derived from the Terra satellite which acquires data every 1–2 days and passes from north to south over the Equator in the morning, while reflectance data are derived from 16-day

composites of MODIS Terra and Aqua satellite products. A summary description of data used is provided in Table 2.

2.5 | Framework of land–atmosphere heat and moisture exchanges

Land–atmosphere interactions are best understood within a surface energy budget (SEB) framework that captures the diagnostic processes responsible for the variation in weather conditions. The SEB expresses the partitioning of net radiation (Q_N , $\text{W}\cdot\text{m}^{-2}$) into sensible (Q_H , $\text{W}\cdot\text{m}^{-2}$) and latent (Q_E , $\text{W}\cdot\text{m}^{-2}$) heat exchanges with the overlying air and heat exchange with the soil (Q_G , $\text{W}\cdot\text{m}^{-2}$),

$$Q_N - Q_G = Q_H + Q_E. \quad (1)$$

Q_N accounts for the radiative factors including short-wave radiation received at ($Q_{S\downarrow}$, $\text{W}\cdot\text{m}^{-2}$), and reflected from ($Q_{S\uparrow}$, $\text{W}\cdot\text{m}^{-2}$) the surface, and longwave radiation received ($Q_{L\downarrow}$, $\text{W}\cdot\text{m}^{-2}$) and emitted ($Q_{L\uparrow}$, $\text{W}\cdot\text{m}^{-2}$), as follows:

$$Q_N = Q_{S\downarrow} - Q_{S\uparrow} + Q_{L\downarrow} - Q_{L\uparrow}. \quad (2)$$

The land surface scheme (LSS) used here simulates the terms of the SEB using routine weather observations and the widely used Monin–Obhukov similarity theory (MOST) (see de Rooy and Holtslag, 1999; Jung *et al.*, 2010; van Heerwaarden *et al.*, 2010; Lu *et al.*, 2014). MOST uses profile relationships of wind, near-surface air temperature, and humidity, to describe the vertical exchanges of momentum, sensible heat (Q_H), and moisture (Q_E), respectively (Paulson, 1970). In addition, the scheme incorporates simplified parameterizations of radiation components (Q_N) and soil heat flux (Q_G), following van Ulden and Holtslag (1985); evapotranspiration is obtained using the Penman–Monteith model (Monteith, 1981). We employ the LSS to simulate hourly surface energy fluxes for mid-day hours (10–15 hr) from May to August, for the period 2010–2019, representing the period when the hourly forcing meteorological data is available. We focus on the mid-day portion of the day when the bulk of the surface–air exchanges associated with vegetated surfaces take place. The application of the LSS approach is fully described in Ishola *et al.* (2020) and the software implementation is available from Ishola *et al.* (2021).

During soil water limiting conditions, Q_E becomes constrained by the surface resistance (r_s), which follows the approach developed by the Jarvis (1976) as

TABLE 2 A summary description of in situ, gridded and satellite-derived data products used in this study

Product	Variable	Resolution (spatial, temporal)	Temporal coverage	Source
In situ	Global solar radiation/sunshine duration, 2-m temperature, relative humidity, m.s.l pressure, wind speed	Hourly	2010–2019	Met Éireann
Gridded	Precipitation	1 km ² , daily	1999–2019	Met Éireann
	ERA5-Land surface volumetric water content (0–7 cm)	0.1°, hourly	1999–2019	Hersbach and Dee (2016)
Satellite	GEOV2 Leaf area index	1 km ² , 10-day	1999–2019	Verger <i>et al.</i> (2014)
	MOD11A1 land surface temperature	1 km, daily	2010–2019	Wan <i>et al.</i> (2015)
	MCD43A4 nadir-adjusted red and near-infrared reflectances	500 m, daily	2010–2019	Schaaf and Wang (2015)

implemented by Beljaars and Bosveld (1997), van de Boer *et al.* (2014) and Ishola *et al.* (2020),

$$r_s = f_r \frac{r_{s,\min}}{\text{LAI}} F_{Q_{s\downarrow}}^{-1} F_{\Delta q}^{-1} F_{\theta}^{-1}, \quad (3a)$$

where f_r is an empirical constant (0.47) and $r_{s,\min}$ is the minimum stomatal resistance (110 s·m⁻¹). The leaf area index (LAI) is set at 2 m²·m⁻²; time-varying LAI values from satellites were not used here due to the coarseness of their spatial resolution, but tests using LAI values between 1 and 3 showed only moderate sensitivity to this parameter at site scale. F represents dimensionless stress functions (ranging from 0–1) which account for the contributions of incoming shortwave radiation ($Q_{s\downarrow}$), atmospheric moisture deficit (Δq), and soil moisture content (θ). $F_{Q_{s\downarrow}}$ is taken as

$$F_{Q_{s\downarrow}} = \frac{Q_{s\downarrow}(S_{rm} - S_r)}{S_{rm}Q_{s\downarrow} + S_r(S_{rm} - 2Q_{s\downarrow})}, \quad (3b)$$

where the empirical coefficients S_{rm} and S_r are 1,000 and 230 W·m⁻². The moisture deficit function is

$$F_{\Delta q} = \frac{1}{(1 + h_s \Delta q)}, \quad (3c)$$

where the empirical coefficient h_s is 0.16 kg·kg⁻¹. The soil moisture function is

$$F_{\theta} = 1 \text{ for } \theta > \theta_{FC}, \quad (3d)$$

$$F_{\theta} = 1 + c_{\text{soil}}(\theta - \theta_{FC}) \text{ for } \theta < \theta_{FC}, \quad (3e)$$

where θ_{FC} (0.3 m³·m⁻³) is the assumed volumetric water content at field capacity. The soil moisture coefficient c_{soil} is taken as 4.3 m³·m⁻³ at all sites (Ishola *et al.*, 2020).

The r_s coefficients used here were previously derived from observations at a number of sites in Ireland where θ measurements were available. However, as the present study employs gridded θ derived from ERA5-Land reanalysis data, the LSS may underestimate r_s and consequently, overestimate Q_E due to potential overestimation of soil water (Dirmeyer *et al.*, 2021) (Figure S1, Supporting Information). We employ a default value for θ_{FC} of 0.3 m³·m⁻³ as there is little information on field capacity across Ireland and this value is similar to that employed in the ERA5-Land model (Balsamo *et al.*, 2009). Despite this simplifying assumption, the general tendency of soil drying and its impact on evapotranspiration should be captured. This is on the basis that soil moisture–evapotranspiration signals are generally recognized to occur below the assumed θ_{FC} value, typically between 50 and 80% of θ_{FC} (e.g., Seneviratne *et al.*, 2010). The parameter c_{soil} has been identified as the key physical property influencing the sensitivity and performance of the LSS (Ishola *et al.*, 2020). We employ the calibrated value (4.3 m³·m⁻³), applied to both wet and seasonally dry soils.

Furthermore, we calculated two biophysical metrics, land surface temperature (T_s) (van de Boer *et al.*, 2014) and evaporative fraction (EF), employing fluxes derived from the LSS as follows:

$$T_s = T_a + \frac{Q_H r_a}{\rho c_p} + z_a \Gamma_d, \quad (4)$$

$$\text{EF} = \frac{Q_E}{Q_N - Q_G}, \quad (5)$$

where T_a is the near-surface temperature, r_a is the aerodynamic resistance, z_a is the reference height, Γ_d is the dry adiabatic lapse rate, ρ is the air density, and c_p is the specific heat capacity of air. These biophysical metrics are important for understanding the role of land–atmosphere feedbacks on extreme weather events such as heatwaves and drought.

2.6 | Data analysis

We initially calculated anomalies (Z-scores) of monthly precipitation, volumetric water content (θ) and LAI for the individual months of May–August, relative to the 1999–2019 period, to place the 2018 summer drought event in the context of previous such events. For the purposes of presenting the results from the LSS, we subsequently grouped the individual 14 AWS stations into broadly representative geographic zones (Figure 1) on the basis of a general definition of agricultural regions (e.g., Green, 2019) and initial evaluation of precipitation. For example, the northwest (Zone A) tends to be wetter, due to its proximity to Atlantic storm tracks, experiences cooler temperature in summer relative to other regions, and has a large proportion of peat soils; the east coast (Zone B) is typically drier, receives more $Q_{S\downarrow}$ and has a high proportion of moderately and well drained soils. Similar to the northwest region, the southwest (Zone C) is also wet but experiences higher average temperatures; soils in this zone are mainly classified as imperfectly or poorly drained. Due to its favourable climate, this zone is dominated by grassland. The “Golden Vale,” a region known for its high-quality dairy production systems, is located within this zone.

Cumulative precipitation and mean deviations of daily θ , vapour pressure deficit (VPD) and LAI were calculated for each zone for the period May–August, relative to 2010–2019. We also applied segmented regression to determine the relationship between daily soil moisture, sensible and latent heat fluxes, employing the evaporative fraction (EF) metric in each zone. The goal here was to identify if critical soil moisture (θ_c) thresholds occurred, and the period during which the θ control of exchange processes became effective. We applied a similar approach using the NIRv data to evaluate and complement the EF based approach; this provides a means of linking θ to vegetation productivity and ecosystem functioning (Buitink *et al.*, 2020).

Segmented regression is used to establish the point at which the linear relationship between an independent (X) and independent variable (Y) changes. This is detected as a breakpoint where there is a significant shift in the slope (sensitivity) representing this relationship. Here, soil moisture (θ) is the independent variable and the surface–atmosphere variables (e.g., EF, NIRv) are the dependent variables,

$$Y = \alpha X + \omega(X - \psi), \quad (6)$$

where ψ is the breakpoint, which represents the critical soil moisture threshold (θ_c), where the response shifts from a wet to dry regime (segments); the dry/left line

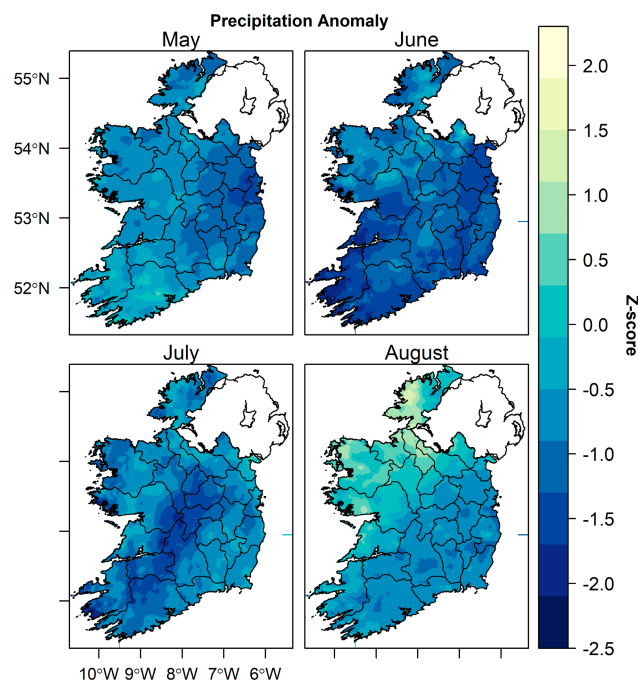


FIGURE 2 Spatial characteristics of monthly precipitation anomaly (z-score) for Ireland during summer 2018, relative to 21-year climatology (1999–2019). Thin lines represent county outlines. The anomalies were calculated from the 1 km gridded precipitation data (Source: Met Éireann) [Colour figure can be viewed at wileyonlinelibrary.com]

($X \leq \psi$) and wet/right line ($X > \psi$) segments have slopes of α and $\beta = \omega + \alpha$, respectively, and ω is the difference-in-slopes. The search for ψ is iterative as the model seeks to find the optimum location for the breakpoint that divides the relationship into two linear segments; the initial value assigned to ψ is 0.25 (based on Seneviratne *et al.*, 2010). Iteration ceases when the model has converged on a solution (Muggeo, 2003). This solution is taken here to be θ_c and distinguishes between the energy- and water-limited states of the surface–air exchanges (Seneviratne *et al.*, 2010). The slope magnitude indicates the severity of dry (hereafter α_{EF} and α_{NIRv})/wet (hereafter β_{EF} and β_{NIRv}) segments (Benson and Dirmeyer, 2020; Buitink *et al.*, 2020) and the transition from one state to another occurs at θ_c . We used the CRAN R “segmented” package to estimate these metrics (Muggeo, 2021).

3 | RESULTS

3.1 | Evolution of 2018 summer drought across Ireland

Figure 2 shows the spatial characteristics of the monthly total precipitation anomalies (Z-score) for the individual

summer months of May–August 2018. Applying the drought categories following McKee *et al.* (1993), the 2018 meteorological drought progressively moved from mild/moderate drought conditions (Z -score of 0 to -1.49) in May to more widespread extreme drought conditions (Z -score < -2.0) in June, evident across the eastern, southern and southwestern part of the country, while conditions in the northwest remained mild/moderate during these months. Rainfall deficits are shown to gradually improve in subsequent months, with the rainfall anomaly in July characterized as moderate drought conditions, with the exception of the midlands; August was characterized by mild drought conditions in the eastern and southern half of the country, with wet conditions (Z -score > 0) in the north and northwest.

To assess the land surface response, the degree of dryness is initially characterized based on anomalies of soil moisture and LAI. The former is based on ERA5-Land which shows reasonable estimates of the available measured soil moisture obtained at three Irish grassland sites, representative of different soil textural characteristics (Figure S1). Figure 3a,b shows the magnitude and spatial extent of ERA5-Land θ and GEOV2-LAI anomalies for the individual months of May–August, 2018. In contrast to the mild/moderate meteorological drought evident in May (Figure 2), soil moisture conditions only begin to deteriorate in June and become exacerbated into July leading to high negative soil moisture anomalies (Z -score < -2.0) being experienced across the entire country, with extreme negative anomalies (Z -score < -3.0) along the usually wet west coast. While the negative θ anomalies were reduced in the north and west during August, the remainder of the country continued to experience significant negative θ anomalies, particularly evident in the south and east of the country (Figure 3a). A strong spatial coherence is also evident between the observed precipitation (Figure 2), ERA5-Land θ and satellite derived GEOV2-LAI (Figure 3a,b) as the meteorological and surface drought characteristics evolve over the study period.

To place these conditions in the context of previous summer drought events, Figure 3c displays the individual monthly (May, June, July and August) anomalies of rainfall, soil moisture (ERA5-Land θ) and LAI (GEOV2) for the period 1999–2019. Although larger rainfall deficits occurred during the 2003 European summer drought, which was one of the driest summers on record (e.g., Casty *et al.*, 2005; Jaksic *et al.*, 2006; Noone *et al.*, 2017), there was no clear impact on vegetation productivity. Thus, the 2003 meteorological drought, while severe, did not develop into agricultural drought across the island, likely related to the timing of the precipitation deficits which occurred in August of that year. In

contrast, due to the timing of the summer 2018 event, both water and vegetation stress conditions are evident, as revealed by the high negative anomalies in precipitation, θ and LAI (Figure 3c). In addition, the largest negative θ and vegetation anomalies in the 21-year record occurred in July 2018, with a negative peak anomaly (Z -score ≈ -2.8) for θ , concurrent with the peak negative anomaly for LAI (Z -score ≈ -1.3).

In the next section, we present the results of the land surface scheme, to explore the perturbations in the surface energy budget associated with the observed surface drying during the summer of 2018.

3.2 | Perturbations of land-atmosphere energy exchanges

To evaluate the robustness of the LSS-derived surface energy fluxes, we initially compared the mid-day observed surface temperature anomaly (relative to 2010–2019), derived from MODIS Terra (for pixels representing the individual weather stations, Figure 1) and the LSS derived surface temperature anomaly (ΔT_s) for the respective stations (Figure 4). Results show high positive ΔT_s for both the Terra and model estimates (peaking at $+5$ to $+10$ K and $+8$ to $+15$ K, respectively) between late June and early July across the selected stations. While the temporal profiles of LSS-derived ΔT_s are largely consistent with the observed Terra ΔT_s , the LSS estimates display a warm bias that can be attributed to an offset in timing between the LSS model estimated values and time of overpass of the satellite; the LSS-derived ΔT_s values are based on the average of the values (from 10:00 to 11:00 hr), while Terra-derived ΔT_s values are based on instantaneous satellite observations at 1030 GMT.

Figure 5 shows the temporal evolution of the in-situ accumulated rainfall (Figure 5a–c), ERA5-Land θ (Figure 5d–f), in situ vapour pressure deficit (VPD) (Figure 5g–i) and satellite-derived LAI (Figure 5j–l) for the period May–August 2018, compared with climatology (1999–2019), for the three zones (A, B, C) previously outlined (Figure 1). The aggregated values are based on the average of the grids corresponding with the station locations, for the gridded data, and station averages for the observed data. In each zone, the cumulative rainfall clearly shows a departure from climatology beginning from just prior to, or around, June 1 (Figure 5a–c). In the northwest (Zone A), the 2018 cumulative rainfall remains closer to climatology, indicating smaller rainfall deficits experienced during June–August, relative to east coast (Zone B) and southwest (Zone C). This is consistent with the gridded precipitation data in Figure 2. The rainfall deficits also begin later in southwest.

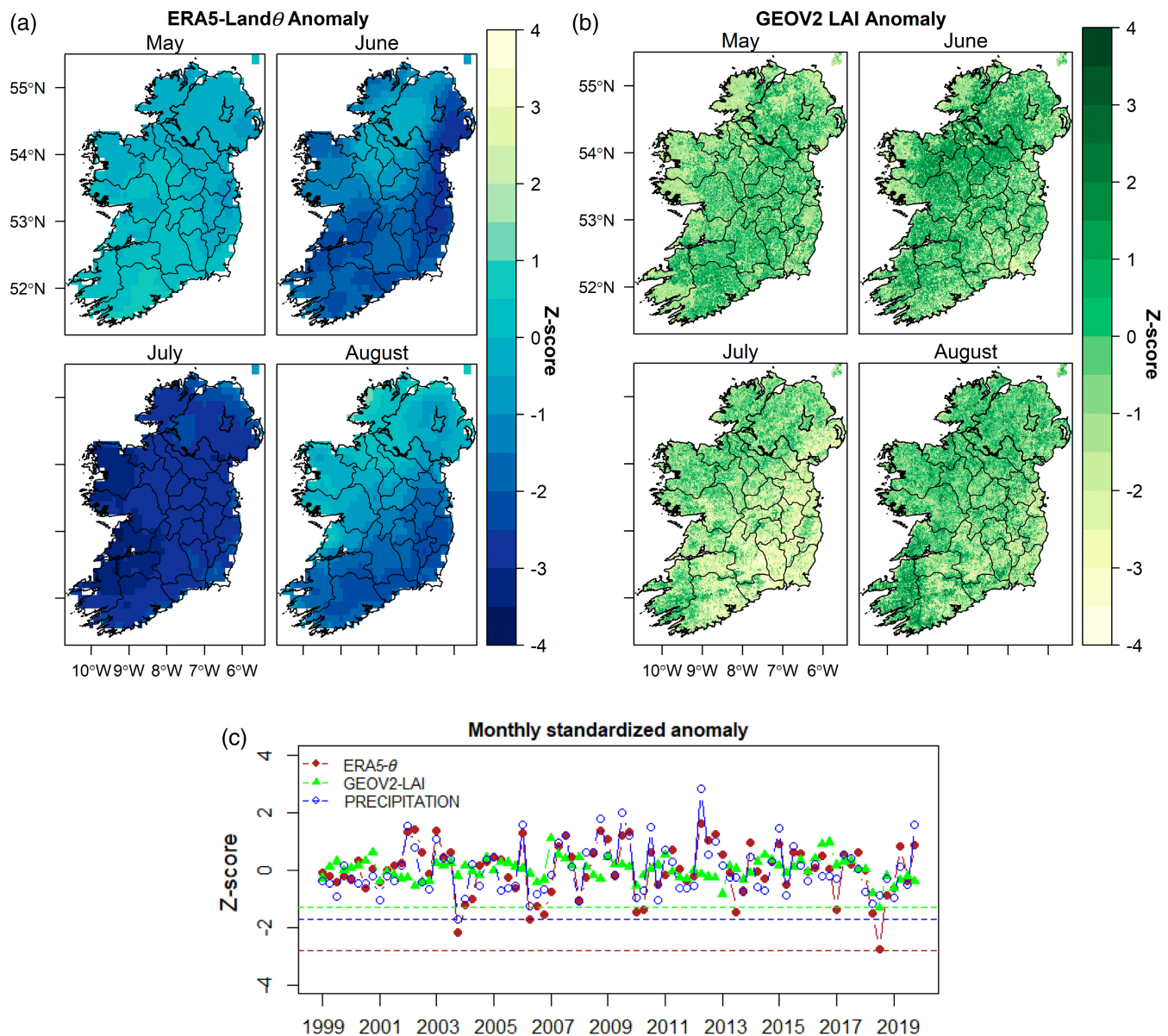


FIGURE 3 Monthly anomalies of ERA5-Land surface soil water content (θ) and satellite-derived GEOV2 leaf area index (LAI) for the individual summer months of 2018, relative to 21-year climatology (1999–2019). (a, b) The spatial characteristics of both parameters; (c) interannual variations of monthly anomalies of θ , LAI and gridded precipitation, averaged over the entire region (blue, red and green horizontal dotted lines show the lowest negative scores for precipitation, θ and LAI, respectively) [Colour figure can be viewed at wileyonlinelibrary.com]

In the northwest, θ losses (Figure 5d) due to evapotranspiration during the start of the season are offset by the normal or above normal rainfall receipts in April and the arrival of Storm Hector in mid-June. Decreasing θ becomes evident from mid-June (approximately 2–3 weeks after the onset of meteorological drought) and reach their lowest negative anomaly (relative to the climatology) of approximately $-0.13 \text{ m}^3 \cdot \text{m}^{-3}$ (40% relative change) around the 4th July. Concurrently, VPD increased from the 21st June and peaks on the 27–28th

June with anomalous values ($>200\%$ relative change) of $+1.0 \text{ kPa}$ (Figure 5g), while LAI shows negligible change during this period (Figure 5j).

For the east of the country, the θ anomaly (relative change), which began earlier than in northwest, is approximately $-0.15 \text{ m}^3 \cdot \text{m}^{-3}$ (50%); this coincides with the highest positive VPD anomaly of $+1.4 \text{ kPa}$ ($>200\%$) and lowest negative anomaly of LAI of $-1.5 \text{ m}^2 \cdot \text{m}^{-2}$, from June 28 (Figure 5e,h,k). The timing of changes in θ , VPD and LAI in the southwest (Figure 5f,i,l) largely

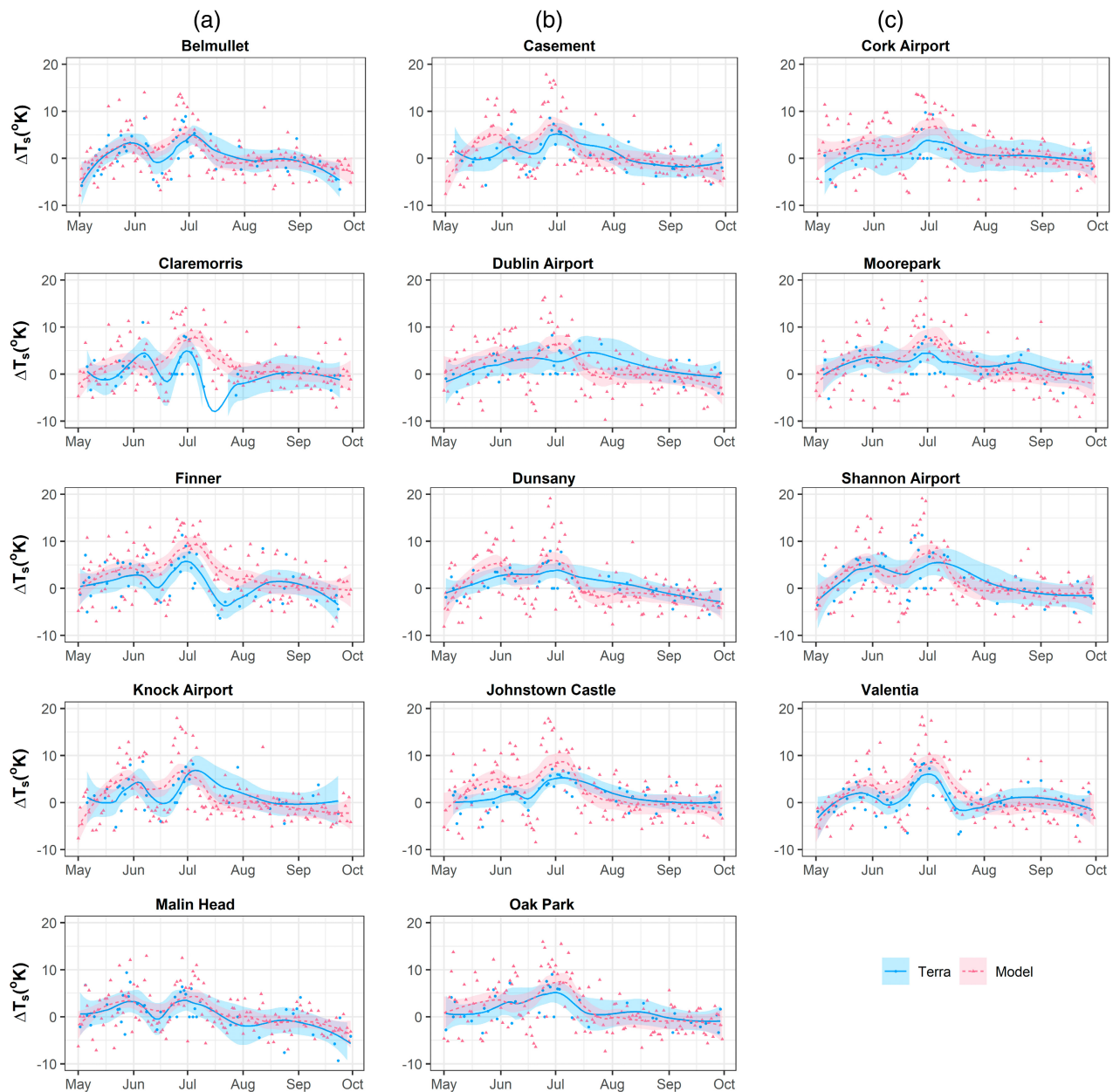


FIGURE 4 Temporal evolution of LSS model-derived (Model) mid-day land surface temperature anomaly (ΔT_s), compared with MODIS Terra (Terra) ΔT_s during 2018 summer, relative to 2010–2019 average across the stations. The lines are derived from smoothed fits of locally weighted polynomial regression (LOESS). The shaded portions represent the 5th and 95th percentiles of uncertainty bounds as calculated by LOESS. The columns under A, B and C indicate stations in each of the previously described zones, as highlighted in Figure 1 and Table 1 [Colour figure can be viewed at wileyonlinelibrary.com]

follow those observed in the east, but slightly lower in magnitude.

The highlighted periods of negative surface (e.g., θ , LAI) and atmospheric (e.g., rainfall, VPD) anomalies (Figure 5) correspond to the LSS-derived periods of higher positive anomalies (relative change) in both the net radiative and energy fluxes. ΔQ_N anomalies of approximately $+200$ to $250 \text{ W}\cdot\text{m}^{-2}$ (180–190%) across the three zones (Figure 6a–c) indicate the strong and

persistent influence of the anticyclonic system, which suppressed cloud formation between June 22 and July 3 across all the zones. Despite the similarity in radiative forcing conditions, anomalies in the mid-day sensible (ΔQ_H) and latent (ΔQ_E) heat fluxes differ across each of the zones, reflecting differences in the partitioning of available energy. For instance, in the northwest, the net radiation surplus gives rise to a latent heat anomaly (ΔQ_E) of $+100$ to $120 \text{ W}\cdot\text{m}^{-2}$ ($\approx 190\%$), largely at the cost

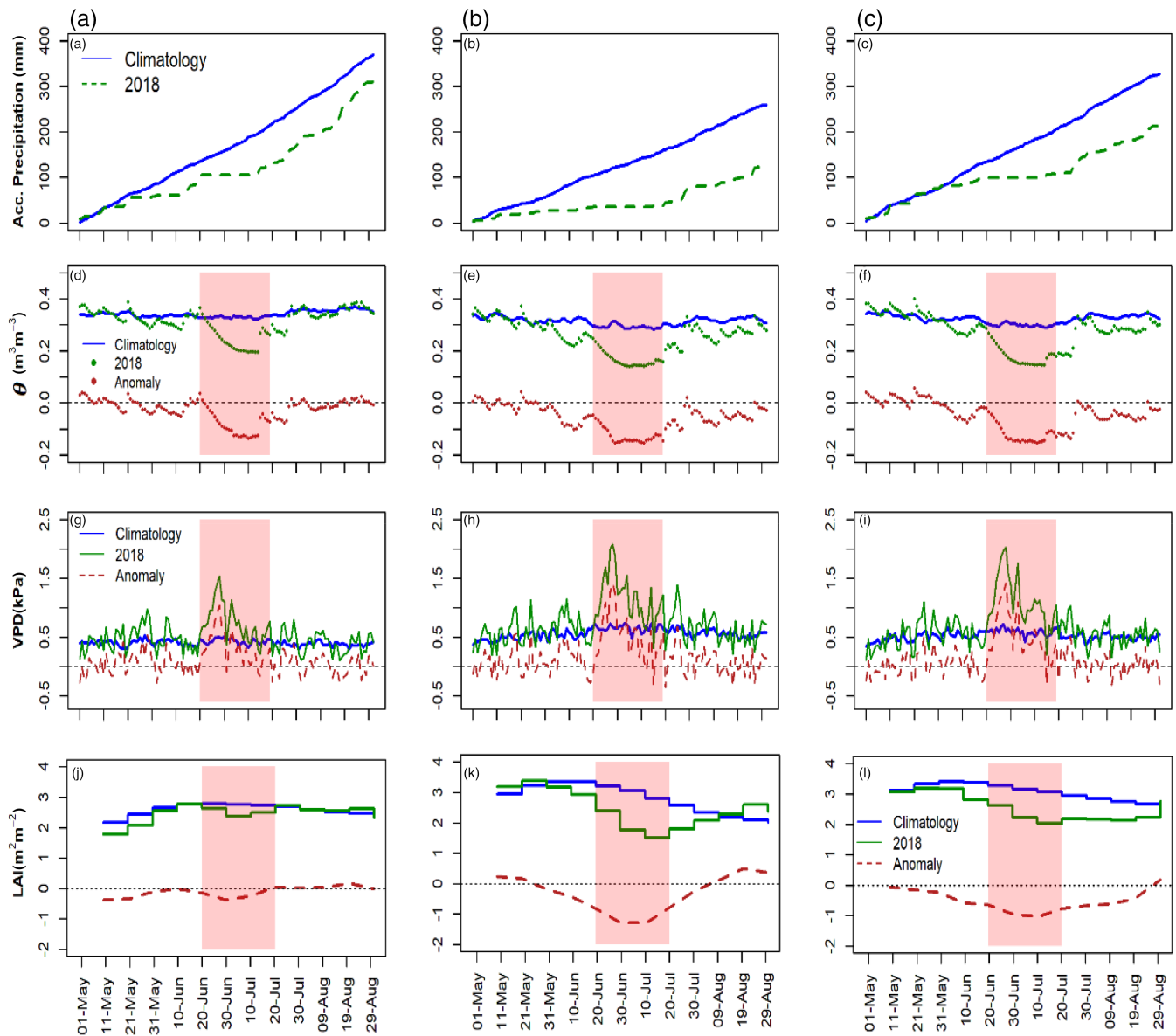


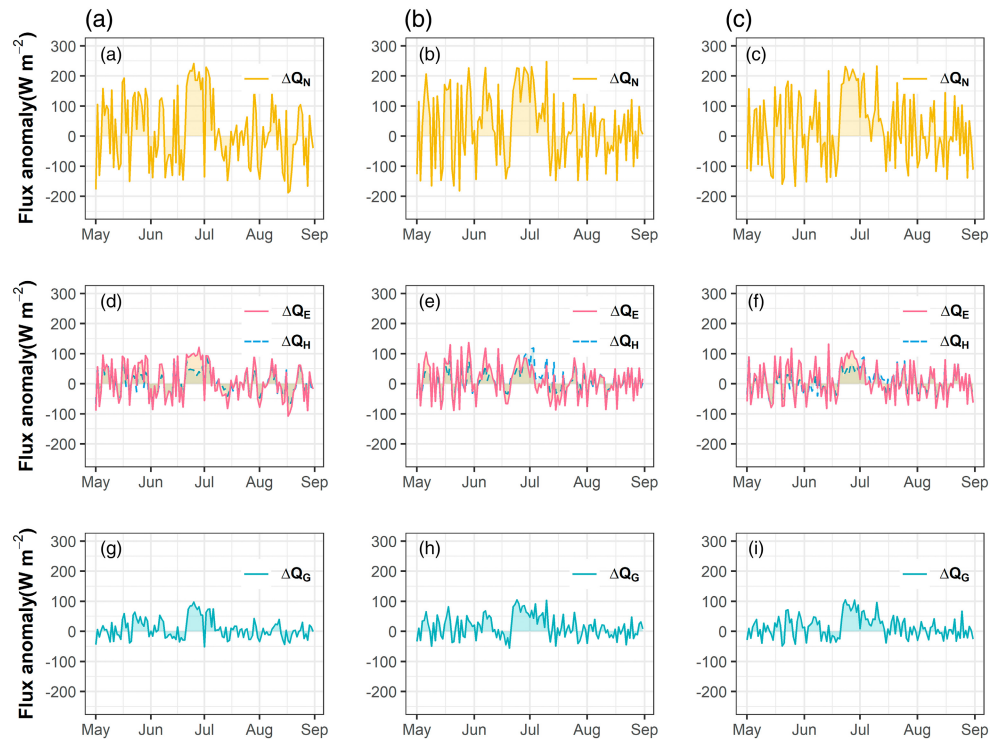
FIGURE 5 Temporal evolution of AWS observed accumulated precipitation (first row), ERA5-Land volumetric water content (second row), in situ vapour pressure deficit (third row) and satellite-derived leaf area index (fourth row); during 2018 summer compared with climatology (1999–2019). Panels A, B and C represent stations in the respective zones highlighted in Figure 1. Values are based on average of stations (and corresponding grids) in each zone. The peach shades represent the observed periods of abnormal surface and atmospheric conditions [Colour figure can be viewed at wileyonlinelibrary.com]

of ΔQ_H . This indicates that plants in this zone were still able to access available soil water, despite the higher ΔQ_N and VPD, between the June 22 and June 30 (Figures 5g and 6a). While the general responses are similar for east and southwest, with the land surface scheme simulating an enhanced positive ΔQ_E anomaly, of $+60$ to $90 \text{ W}\cdot\text{m}^{-2}$ (140–190%) and $+50$ to $100 \text{ W}\cdot\text{m}^{-2}$ (130–170%), respectively (Figure 6e,f). However, by the end of June, ΔQ_H exceeds ΔQ_E in the east and ΔQ_H is equivalent to ΔQ_E in southwest, providing evidence of a land–atmosphere feedback, evident in the enhanced VPD

(Figure 5h,i), relative to northwest (Figure 5g), starting from June 27 in the east (Figure 6e) and July 1 in southwest (Figure 6f).

Overall, these results show enhanced Q_E , well above normal, caused by high positive anomalies of ΔQ_N prior to the 27th June. The observed changes between late June and early July in the east and southwest highlight the differentiating role of plant available soil moisture and support the divergent landscape physiological responses (e.g., LAI; Figure 3b) to atmospheric anomalies relative to the northwest.

FIGURE 6 Temporal evolution of model-derived mid-day anomalous net radiative flux (ΔQ_N) (first row), sensible heat (ΔQ_H) and latent heat (ΔQ_E) fluxes (second row) and soil heat flux (ΔQ_G) (third row), during 2018 summer, relative to analysis period (2010–2019). Panels A, B and C are for stations in the respective zones highlighted in Figure 1. Values represent the day time (1000–1500 GMT) average [Colour figure can be viewed at wileyonlinelibrary.com]



3.3 | Relationship between soil moisture and surface flux densities

To further explore the role of soil moisture availability in drought evolution, we used segmented regression to examine the relationships between daily ERA5-Land θ and anomalies of EF and NIRv (Figure 7), and separately for ΔQ_E and ΔQ_H (Figure S2) for each zone. The results for individual stations are provided in Table S1. It should be noted that the results here are exploratory and based on a LSS specified θ_{FC} value ($0.3 \text{ m}^3 \cdot \text{m}^{-3}$) (as outlined in section 2.5).

While the models detect a breakpoint (critical θ threshold, $\theta_c \approx 0.36 \text{ m}^3 \cdot \text{m}^{-3}$) separating wet and dry regime in the northwest zone (Figure 7a), the α_{EF} sensitivity in the dry segment is insignificant and close to 0. In contrast, the θ -NIRv approach identified a critical θ threshold (θ_c) $\approx 0.30 \text{ m}^3 \cdot \text{m}^{-3}$ with a higher α_{NIRv} sensitivity indicated in the dry segment (adjusted $R^2 = 0.60$, p -value = 2.27×10^{-12}) (Figure 7d). This indicates that the landscapes in the northwest largely sustain the conditions in which changes in EF is independent of θ , whereas the NIRv signal is influenced by θ during the summer season.

However, the θ -EF relationship is clearly captured in the east (Figure 7b,e) where the approach identified a critical threshold θ_c of $\approx 0.18 \text{ m}^3 \cdot \text{m}^{-3}$, a value that is likely close to the wilting point. The sensitivity ($\beta_{EF} \approx 0$) is negligible in the wet segment, but a significant and steep α_{EF} slope is observed in the dry segment (adjusted $R^2 = 0.29$, p -value = .039), indicating that EF is constrained and

linearly coupled with the surface during the period when θ is below the critical point. Findings are consistent for the θ -NIRv approach ($\theta_c = 0.23 \text{ m}^3 \cdot \text{m}^{-3}$ and adjusted $R^2 = 0.77$, p -value = 2.44×10^{-12}).

The results of this exploratory analysis in the southwest identify a critical θ threshold (θ_c) $\approx 0.35 \text{ m}^3 \cdot \text{m}^{-3}$, similar to northwest, but with a significantly (p -value = 2.59×10^{-7}) higher α_{EF} sensitivity in the dry segment (adjusted $R^2 = 0.23$) (Figure 7c). Comparing with the θ -NIRv approach, the α_{NIRv} sensitivity is similar (adjusted $R^2 = 0.32$) but with a higher estimate ($0.35 \text{ m}^3 \cdot \text{m}^{-3}$, p -value = .000125) of θ_c (Figure 7f).

Both the EF and NIRv approaches agree on the coupling for the east and southwest; however, the differences in estimated θ_c suggest causality in θ -EF framework (e.g., soil type) that may not be inferred using statistical regression analysis. Independent assessments based on the relationship between ERA5-Land θ and model-derived Q_H and Q_E fluxes (Figure S2) show that Q_H is the major mechanistic factor driving the θ -EF signals, and likely responsible for the increased atmospheric sensitivity that contributed to occurrence of the abnormally warm and dry days during summer 2018, as revealed in the east and southwest.

4 | DISCUSSION

In this study, we evaluated the use of a land surface scheme that employed readily available meteorological

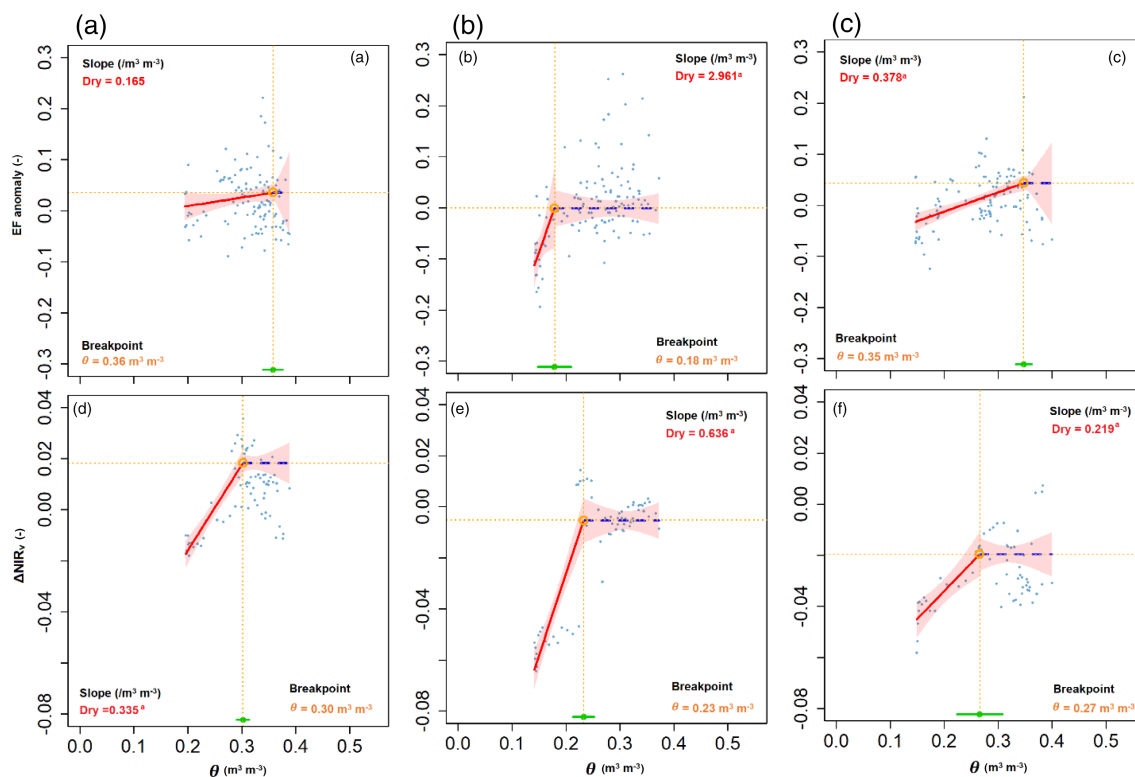


FIGURE 7 Relationships between soil moisture (θ), evaporative fraction (EF) [first row] and MODIS NIRv [second row], based on segmented regression analysis during 2018 summer across the zones. The thick red lines are measures of sensitivity (slope) on the dry segment while dashed blue lines are for wet segment. The dashed orange lines show the θ -EF and θ -NIRv breakpoints and the horizontal green lines at the bottom show the confidence interval of θ breakpoints. Significant at p -value $< .05$. Panels A, B and C are for stations in the respective zones highlighted in Figure 1 [Colour figure can be viewed at [wileyonlinelibrary.com](https://onlinelibrary.wiley.com/doi/10.1002/joc.7785)]

data to assess the impact of the 2018 summer drought on regional land-atmosphere heat and moisture exchanges. The performance of the scheme was evaluated in comparison with MODIS-derived surface temperature anomalies (ΔT_s) with results that are consistent with the findings of Zaitchik *et al.* (2006) who showed similar timing and distribution of spikes in ΔT_s between MODIS-derived and model estimates from NCEP/NCAR reanalyses for the summer 2003 drought in France. This supports the argument that Ireland experienced a compound drought event where land-atmosphere feedbacks enhanced its severity. Understanding of the response of the vegetation to these events is limited (e.g., Streck, 2003; Teuling, 2018), but is important in assessing agricultural productivity.

4.1 | Changes in land surface processes during severe drought

During extreme weather events such as drought, perturbations in the surface energy budget drive changes in near-surface temperature and reductions in available soil water. In soils with limited available soil water, plant

water uptake to meet the increasing atmospheric evaporative demand will be restricted (Teuling, 2018), as a result, available Q_N will be converted to Q_H flux. This positive feedback on Q_H can act to amplify drought characteristics. The perturbations of surface exchanges of heat and moisture which impact the patterns of atmospheric temperature are mediated through changes in θ (Seneviratne *et al.*, 2010; Miralles *et al.*, 2014).

The analysis of the 2018 event indicates that an increase in net radiative fluxes (ΔQ_N) was evident from May to July and this was associated with decreasing θ and increasing VPD (Figure 5d-i). LAI response to the changing land surface conditions was evident in the east, southeast and southwest zones (Figure 5k,l). While the northwest displayed an increase in VPD and decline in θ over this period; the vegetation response was less marked in the LAI response (Figures 3b and 5j), relative to the climatology, for this region. The mild drought conditions experienced in the northwest during June, relative to the rest of the country, were associated with the passage of a rainstorm in mid-June (Met Éireann Report, 2018). In general, the observed magnitude, extent and timing of the 2018 meteorological drought are in agreement with those reported by Falzoi *et al.* (2019). The LSS analysis

shows that Q_N was largely partitioned into Q_E rather than Q_H during this period in the northwest, which is typical of grasslands even under extremely warm temperatures (Lansu *et al.*, 2020; Stap *et al.*, 2014; Teuling *et al.*, 2010; van Heerwaarden and Teuling, 2014) where soil water remains available to plants. The partitioning of available energy into Q_E is similar for the east and the southwest, but with lower magnitude Q_E anomalies. This enhancement of Q_E even under water-limited conditions was likely facilitated by the integrated effects of higher downward shortwave radiation and increased VPD. However, the ratio between Q_E and Q_H in the east and southwest indicates that a greater proportion of Q_N was channelled into Q_H and this is apparent in the negative anomalies of LAI in these zones during the month of June (Figure 3b). The shift from latent to sensible heat and reduction in LAI during June and July indicate decreasing θ , and hence vegetation stress in the region (Figure 5e).

The impact on vegetation response, represented by anomalies in GEOV2 LAI, closely tracked the evolving θ conditions (Figure 3b). These findings are consistent with those of Albergel *et al.* (2019) who found similar perturbations (index >-1.0 and -2.0) in surface θ during the month of July in the United Kingdom. Based on our analysis, grassland in the east responded faster to meteorological drought conditions than elsewhere. Several contributing factors are likely to explain this; the southeast is characterized by relatively well drained soils and can experience seasonal θ deficits during “normal” years. April 2018 experienced average, or above average, rainfall at most stations; where soils have storage capacity, such as the imperfectly or poorly drained soils more typical of the southwest and northwest, the additional water offset evaporative losses. Rain in June resulted in θ returning to normal levels in the northwest (Figure 5d) and southwest (Figure 5f). Soil drying was more advanced in the east (Figure 5e) and increased due to high Q_E during June (Figure 6b) with a marked response in vegetation, evident in the negative anomalies of LAI, during June. By July, with increased plant stress due to the reduction in θ , the positive Q_N anomaly is expended as Q_H and Q_G , warming the atmosphere, increasing water demand and exacerbating soil moisture and vegetation. A similar reasoning applies to the southwest based on the LSS simulated fluxes (Figure 6c) and is supported by the increasing negative anomalies in LAI in the zone during this month. The drought response of grasslands is shown to be dependent on the antecedent conditions, geographical area and soil characteristics (findings consistent with Xiao *et al.* (2009) and Zhang *et al.* (2012)).

Although time varying GEOV2 LAI values are not integrated within the current modelling framework,

altering the LAI value between 1 and 3 $\text{m}^2 \cdot \text{m}^2$ in Equation (3a), the range in values observed during the study period, was found to have only a moderate impact on the estimated evaporative flux. A fixed LAI value of 2 $\text{m}^2 \cdot \text{m}^2$ was therefore utilized. Nonetheless, we recognize the potential of incorporating more representative higher spatial, and temporal, resolution satellite observations of LAI (e.g., Sentinel-2) to improve the representation of field scale vegetation dynamics within the modelling framework.

The positive anomalous ΔQ_H and ΔQ_E are largely correlated with an increase in net radiative flux during early summer but in the east, the negative ΔQ_E values in July can be explained by increasing water-stress conditions in the root zone of grasses. This zone is distinguished by its free-draining soils (Creamer *et al.*, 2014) that makes it especially vulnerable to meteorological drought conditions, if they occur during the growing season (e.g., 2003 vs. 2018; Figure 3c).

4.2 | Role of soil moisture in land-atmosphere exchanges during 2018 summer

Soil moisture (θ) can significantly influence terrestrial water, energy, and carbon cycling through its control on Q_E at the land-atmosphere interface. This connection can be explored using a soil moisture-evaporative fraction (θ -EF) framework that distinguishes the transition from wet to dry evaporative regime: (a) a wet regime in which EF is independent of θ and (b) a dry regime where θ and EF are linearly coupled. The critical soil moisture content (widely referred to as critical soil moisture thresholds) that separate these regimes is important as it can help identify the mechanisms responsible for the shift from a normal into a water-stress regime, where the land surface state controls the sensitivity of the atmosphere (Seneviratne *et al.*, 2010).

We applied segmented regression analysis on the ERA5-Land θ and estimated EF anomaly to identify the threshold in soil moisture (θ_c) that marks the transition from wet to dry regime; a similar approach was applied to the NIRv data. The estimated θ_c values are identical to those derived using measured θ deeper in the soil layer, from two sites in the Netherlands (Buitink *et al.*, 2020). Hence, these findings suggest that drying soils increase the sensitivity of land-atmosphere coupling, in turn aggravating the surface drying, based on ERA5-Land θ (note that ERA5-Land underestimates very dry soils for a number of Irish sites). In the east, this shift was identified as occurring in late June (≈ 22 nd June), indicating the onset of agricultural drought. The dry regime was

sustained for several days (20) during which θ -EF are linearly coupled demonstrating the “hypersensitive” response of this region to meteorological droughts. In a previous study over grassland above saturated soils in the south of Ireland, Jaksic *et al.* (2006) reported that measured θ status in both dry and wet years are different, but well above wilting point, so that the impact of θ status on net ecosystem functioning is small and identical for both years. This is consistent with our findings over the north-west where the landscape either shows no α_{EF} sensitivity or the θ -EF coupling is too weak to support the theoretical θ -EF framework (Seneviratne *et al.*, 2010). Results of α_{EF} in the southwest also indicated a weak θ -EF coupling; however, the land surface response to reduced θ is evident in the vegetation response (Figure 3b)—further work is necessary to explore this. The differing land responses, as reflected in different estimated θ_c values, also suggest the local effects of predominant soil types across the zones. The zones are characterized by different soil properties (Creamer *et al.*, 2014), in essence, the reinforcement of soil moisture-evaporation signal, which is distinguished by θ_c , partly depends on the nature of the soil and its water holding ability.

A further assessment indicates that the signal in EF is largely driven by Q_H during the dry regimes, as revealed in the east (Figure S2). Therefore, Q_H appears to be the mechanistic factor responsible for the unusual shift in land-atmosphere coupling and consequently amplified agricultural drought during summer 2018.

ERA5-Land uses monthly climatology of LAI to generate the global reanalyses data (Boussetta *et al.*, 2013), which may contribute to weak θ -EF signals in these zones. There is the possibility that ERA5-Land may have underestimate very dry soils as demonstrated in Figure S1, consequently resulting in the LSS to underestimate the impact of soil moisture anomalies on land-atmosphere feedback mechanisms. The offsets between measured and ERA5-Land θ values are largely represented in values below $0.25 \text{ m}^3 \cdot \text{m}^{-3}$. It should also be noted that the ERA5-Land θ at the surface soil layer was evaluated with measured θ at the deeper soil layer (20 cm) across the sites. The surface θ derived from models or satellites are thought to decouple from θ in the deeper soil profile where plants may take up water depending on root density, and consequently may not explain the dynamics of processes in the root zone (Buitink *et al.*, 2020). However, the choice of ERA5-Land surface θ to diagnose drought processes, as in recent studies (Benson and Dirmeyer, 2020; Dirmeyer *et al.*, 2021), is on the basis that θ anomalies develop progressively down deeper soil layers during a drought event, as plants increase water uptake from near the surface to the sub-surface. Thus, θ values may further lead to larger offsets

under $0.25 \text{ m}^3 \cdot \text{m}^{-3}$, since the θ at the deeper layers are always higher than at the upper soil layers. This is consistent with Dirmeyer *et al.* (2021) who noted that ERA5-Land underestimates the impact of very dry soils on extreme temperatures, over Britain in 2018 summer. Finally, the assumed volumetric water content at field capacity (θ_{FC}) of $0.3 \text{ m}^3 \cdot \text{m}^{-3}$, necessary to apply the LSS in the absence of measured θ_{FC} , may also have contributed.

5 | CONCLUSION

Here, we evaluated the use of a physically based land surface scheme, in combination with readily available ERA5-land global reanalyses surface soil moisture data and ground-based meteorology, to estimate the surface flux densities and evaporative fraction (EF) to understand the land surface response to the atmospheric forcing during the summer of 2018. The approach allows us to explore changes in land surface processes and the effect of a soil moisture regime shift on land-atmosphere sensitivities. We demonstrate the application of this framework, utilizing data from 14 weather stations distributed across Ireland, during the 2018 summer record-breaking heat and drought events.

The study revealed synoptic timescale variability in anomalous land-atmosphere heat and moisture transfers, across the stations and between dates. Drought-induced perturbations in land surface processes are largely not effective until the period between late June/early July and extend to mid-July in some cases. Prior to this period, the processes were constrained by atmospheric anomalies. That is, in the absence of rainfall, the higher evaporative demand due to warmer temperature enhanced latent heat flux (Q_E) via increase in evapotranspiration rates, leading to the higher soil moisture deficits in July across the country. This is particularly apparent in the east and southeast regions, where drying soils quickly shifted the landscape into a “dry” regime in which EF is self-limiting, consequently providing a positive land-atmosphere feedback mechanism (increase in land surface temperature and Q_H), beginning from the 27th June and further exacerbated agricultural drought in July.

Segmented regression analysis of θ -EF interplay has found significant critical soil moisture threshold ($\theta_c \approx 0.18 \text{ m}^3 \cdot \text{m}^{-3}$, and $\theta_c \approx 0.23 \text{ m}^3 \cdot \text{m}^{-3}$ for θ -NIRv analysis) at which land-atmosphere signals potentially become hypersensitive in the east and southeast zone, based on ERA5-Land. These values also represent the point of onset of drought impact on landscapes and ecosystem functioning in this region. Although, the segmented models also identified soil moisture shift across

the rest of the country, the linear θ -EF coupling was too weak to conclude that EF was constrained by land surface state in these areas. While spatial variations in precipitation and local effects of soil and vegetation structures may play a critical role in the differing land responses, it should be noted that ERA5-Land underestimates seasonally dry soil moisture regimes for Irish landscapes, which may have broadly informed less and inconsistent impact of soil moisture anomalies on the exchange processes across the region.

Nonetheless, the findings of this study are invaluable to speculate the zones and critical soil moisture values under which land-atmosphere exchanges are constrained by the land surface state and further exacerbate surface warming and dryness. This contribution is important, certainly for Ireland, not only because it may help improve the representation of soil moisture factors in Numerical Weather Prediction (NWP) models, but can also help to enhance sub seasonal predictability of drought propagation and early warning systems of summer climate extremes in the future episodes.

ACKNOWLEDGEMENTS

This study was supported by the Teagasc Irish Agriculture and Food Development Authority under the Walsh Fellowship Programme (Project Number: 2016076). The authors are grateful to Met Éireann, the Irish Meteorological Service, for providing routine weather observations and gridded precipitation. The ERA5-Land soil moisture data are obtained from <https://cds.climate.copernicus.eu/>, and MODIS products are available from https://lpdaac.usgs.gov/product_search/. The satellite-derived GEOV2-LAI data are obtained from <https://land.copernicus.eu/>. We thank the anonymous reviewers for their invaluable comments and suggestions. The python code used for flux simulations is available from https://zenodo.org/record/4679843#.YQLf_I5Khpk. Open access funding provided by IREL.

CONFLICT OF INTEREST

The authors declare no potential conflict of interest.

ORCID

Kazeem A. Ishola  <https://orcid.org/0000-0003-3264-0910>

REFERENCES

- Akbar, R., Short Gianotti, D.J., McColl, K.A., Haghghi, E., Salvucci, G.D. and Entekhabi, D. (2018) Estimation of landscape soil water losses from satellite observations of soil moisture. *Journal of Hydrometeorology*, 19, 871–889.
- Albergel, C., Dutra, E., Bonan, B., Zheng, Y., Munier, S., Balsamo, G., de Rosnay, P., Muñoz-Sabater, J. and Calvet, J.-C. (2019) Monitoring and forecasting the impact of the 2018

- summer heatwave on vegetation. *Remote Sensing*, 11, 520. <https://doi.org/10.3390/rs11050520>.
- Alexander, L. (2011) Climate science: extreme heat rooted in dry soils. *Nature Geoscience*, 4, 12–13. <https://doi.org/10.1038/ngeo1045>.
- Allen, R.G., Pereira, L.S., Raes, D. and Smith, M. (1998) Crop evapotranspiration. In: *Guidelines for Computing Crop Water Requirements*. Irrigation and Drainage Paper No. 56. Rome: FAO.
- Badgley, G., Anderegg, L.D.L., Berry, J.A. and Field, C.B. (2019) Terrestrial gross primary production: using NIRV to scale from site to globe. *Global Change Biology*, 25, 3731–3740. <https://doi.org/10.1111/gcb.147299>.
- Badgley, G., Field, C.B. and Berry, J.A. (2017) Canopy near-infrared reflectance and terrestrial photosynthesis. *Science Advances*, 3, e1602244. <https://doi.org/10.1126/sciadv.1602244>.
- Baldocchi, D.D., Ryu, Y., Dechant, B., Eichelmann, E., Hemes, K., Ma, S., Sanchez, C.R., Shortt, R., Szutu, D., Valach, A., Verfaillie, J., Badgley, G., Zeng, Y. and Berry, J.A. (2020) Outgoing near infrared radiation from vegetation scales with canopy photosynthesis across a spectrum of function, structure, physiological capacity and weather. *Journal of Geophysical Research: Biogeosciences*, 125, e2019JG005534. <https://doi.org/10.1029/2019JG005534>.
- Balsamo, G., Viterbo, P., Beljaars, A., van den Hurk, B., Hirschi, M., Betts, A.K. and Scipal, K. (2009) A revised hydrology for the ECMWF model: verification from field site to terrestrial water storage and impact in the integrated forecast system. *Journal of Hydrometeorology*, 10, 623–643.
- Baret, F., Weiss, M., Lacaze, R., Camacho, F., Makhmarad, H., Pacholczyk, P. and Smetse, B. (2013) GEOV1: LAI, FAPAR essential climate variables and FCOVER global time series capitalizing over existing products, part 1: principles of development and production. *Remote Sensing of Environment*, 137, 299–309.
- Beljaars, A.C.M. and Bosveld, F.C. (1997) Cabauw data for the validation of land surface parameterization schemes. *Journal of Climate*, 10, 1172–1193.
- Benson, D.O. and Dirmeyer, P.A. (2020) Characterizing the relationship between temperature and soilmoisture extremes and their role in the exacerbation of heatwaves over the contiguous United States. *Journal of Climate*, 34(6), 2175–2187.
- Black, E., Blackburn, M., Harrison, G., Hoskins, B. and Methven, J. (2004) Factors contributing to the summer 2003 European heatwave. *Weather*, 59, 217–223. <https://doi.org/10.1256/wea.74.04>.
- Boussetta, S., Balsamo, G., Beljaars, A., Kral, T. and Jarlan, L. (2013) Impact of a satellite-derived leaf area index monthly climatology in a global numerical weather prediction model. *International Journal of Remote Sensing*, 34(9–10), 3520–3542. <https://doi.org/10.1080/01431161.2012.716543>.
- Buitink, J., Swank, A.M., van der Ploeg, M., Smith, N.E., Benninga, H.-J.F., van der Bolt, F., Carranza, C.D.U., Koren, G., van der Velde, R. and Teuling, A.J. (2020) Anatomy of the 2018 agricultural drought in the Netherlands using in situ soil moisture and satellite vegetation indices. *Hydrology and Earth System Sciences*, 24, 6021–6031. <https://doi.org/10.5194/hess-24-6021-2020>.
- Buras, A., Rammig, A. and Zang, C.S. (2019) Quantifying impacts of the drought 2018 on European ecosystems in comparison to 2003. *Biogeosciences*, 17, 1655–1672.
- Casty, C., Wanner, H., Luterbacher, J., Esper, J. and Böhm, R. (2005) Temperature and precipitation variability in the

- European Alps since 1500. *International Journal of Climatology*, 25, 1855–1880. <https://doi.org/10.1002/joc.1216>.
- Conti, S., Meli, P., Minelli, G., Solimini, R., Toccaceli, V., Vichi, M., Beltrano, C. and Perini, L. (2005) Epidemiologic study of mortality during the summer 2003 heat wave in Italy. *Environmental Research*, 98, 390–399.
- Creamer, R.E., Simo, I., Reidy Carvalho, J., Fealy, R., Hallett, S., Jones, R., Holden, 829.A., Holden, N., Hannam, J., Massey, P., Mayr, T., McDonald, E., O'Rourke, S., Sills, P., Truckell, I., Zawadzka, J. and Schulte, R.P.O. (2014) *Irish Soil Information System*. Wexford: EPA STRIVE Programme. Synthesis report (2007-S-CD-1-S1).
- de Rooy, W.C. and Hultsag, A.A.M. (1999) Estimation of surface radiation and energy flux densities from single-level weather data. *Journal of Applied Meteorology*, 38, 526–540.
- Denissen, J.M., Teuling, A.J., Reichstein, M. and Orth, R. (2020) Critical soil moisture derived from satellite observations over Europe. *Journal of Geophysical Research: Atmospheres*, 125, e2019.
- Denissen, J.M.C., Orth, R., Wouters, H., Miralles, D.G., van Heerwaarden, C.C., de Arellano, J.V.-G. and Teuling, A.J. (2021) Soil moisture signature in global weather balloon soundings. *npj Climate and Atmospheric Science*, 4, 13.
- Dillon, E., Moran, B., Lennon, J. and Donnellan, T. (2018) *Teagasc National Farm Survey 2018 Results*. Available at: <https://www.teagasc.ie/publications/2019/National-Farm-Survey-Preliminary-Results-2018.php> [Accessed November, 2019].
- Dirmeyer, P.A., Balsamo, G., Blyth, E.M., Morrison, R. and Cooper, H.M. (2021) Land-atmosphere interactions exacerbated the drought and heatwave over northern Europe during summer 2018. *AGU Advances*, 2, e2020AV000283. <https://doi.org/10.1029/2020AV000283>.
- Dole, R., Hoerling, M., Perlwitz, J., Eischeid, J., Pegion, P., Zhang, T., Quan, X.-W., Xu, T. and Murray, D. (2011) Was there a basis for anticipating the 2010 Russian heat wave? *Geophysical Research Letters*, 38, L06702. <https://doi.org/10.1029/2010GL046582>.
- Falzo, S., Gleeson, E., Lambkin, K., Zimmermann, J., Marwaha, R., O'Hara, R., Green, S. and Fratianni, S. (2019) Analysis of the severe drought in Ireland in 2018. *Weather*, 99(99), 1–6. <https://doi.org/10.1002/wea.3587>.
- Feldman, A.F., Short Gianotti, D.J., Trigo, I.F., Salvucci, G.D. and Entekhabi, D. (2019) Satellite-based assessment of land surface energy partitioning-soil moisture relationships and effect of confounding variables. *Water Resources Research*, 55, 10657–10677.
- Fink, A.H., Brücher, T., Krüger, A., Leckebusch, G.C., Pinto, J.G. and Ulbrich, U. (2004) The 2003 European summer heatwaves and drought—synoptic diagnosis and impacts. *Weather*, 59, 209–216.
- García-Herrera, R., Díaz, J., Trigo, R.M., Luterbacher, J. and Fischer, E.M. (2010) A review of the European summer heatwave of 2003. *Critical Reviews in Environmental Science and Technology*, 40, 267–306.
- Green, S. (2019) *Investigation into the bio-physical constraints on farmer turn-out-date decisions using remote sensing and meteorological data*. PhD thesis, University College Cork. Available at: <http://hdl.handle.net/10468/7795>.
- Haghighi, E., Short Gianotti, D.J., Akbar, R., Salvucci, G.D. and Entekhabi, D. (2018) Soil and atmospheric controls on the land surface energy balance: a generalized framework for distinguishing moisture-limited and energy-limited evaporation regimes. *Water Resources Research*, 54, 1831–1851.
- Hersbach, H. and Dee, D. (2016) ERA-5 reanalysis is in production. *ECMWF Newsletter*, 147, 7.
- Ishola, K. A., Fealy, R. and Mills, G. (2021) SURFLEX (version v1.1.0). Zenodo. <https://doi.org/10.5281/zenodo.4679843>
- Ishola, K.A., Fealy, R., Mills, G., Fealy, R., Green, S., Jimenez-Casteneda, A. and Adeyeri, O.E. (2018) Developing regional calibration coefficients for estimation of hourly global solar radiation in Ireland. *International Journal of Sustainable Energy*, 38(3), 297–311. <https://doi.org/10.1080/14786451.2018.1499645>.
- Ishola, K.A., Mills, G., Fealy, R.M., Ní, C.Ó. and Fealy, R. (2020) Improving a land surface scheme for estimating sensible and latent heat fluxes above grassland with contrasting soil moisture zones. *Agricultural and Forest Meteorology*, 294, 108151. <https://doi.org/10.1016/j.agrformet.2020.108151>.
- Jaksic, V., Kiely, G., Albertson, J., Oren, R., Katul, G., Leahy, P. and Byrne, K.A. (2006) Net ecosystem exchange of grassland in contrasting wet and dry years. *Agricultural and Forest Meteorology*, 139, 323–334.
- Jarvis, P. (1976) The interpretation of leaf water potential and stomatal conductance found in canopies in the field. *Philosophical Transactions of the Royal Society B*, 273, 593–610.
- Jung, M., Reichstein, M., Ciais, P., Seneviratne, S.I., Sheffield, J., Goulden, M.L., Bonan, G., Cescatti, A., Chen, J., de Jeu, R., Dolman, A.J., Eugster, W., Gerten, D., Gianelle, D., Gobron, N., Heinke, J., Kimball, J., Law, B.E., Montagnani, L., Mu, Q., Mueller, B., Oleson, K., Papale, D., Richardson, A.D., Rouspard, O., Running, S., Tomelleri, E., Viovy, N., Weber, U., Williams, C., Wood, E., Zaehle, S. and Zhang, K. (2010) Recent decline in the global land evapotranspiration trend due to limited moisture supply. *Nature*, 467, 951–954.
- Keane, T. and Collins, J.F. (2004) *Climate, Weather and Irish Agriculture*. Dublin: AGMET, UCD, p. 4.
- Knist, S., Goergen, K., Buonomo, E., Christensen, O.B., Colette, A., Cardoso, R.M., Fealy, R., Fernandez, J., Garcia-Diez, M., Jacob, D., Kartsios, S., Katragkou, E., Mayer, S., van Meijgaard, E., Nikulin, G., Soares, P.M.M., Sobolowski, S., Szepszo, G., Teichmann, C., Vautard, R., Warrach-Sagi, K., Wulfmeyer, V. and Simmer, C. (2017) Land atmosphere coupling in EURO-CORDEX evaluation experiments. *Journal of Geophysical Research: Atmospheres*, 122, 79–103.
- Kornhuber, K., Osprey, S., Coumou, D., Petri, S., Petoukhov, V., Rahmstorf, S. and Gray, L. (2019) Extreme weather events in early summer 2018 connected by a recurrent hemispheric wave-7 pattern. *Environmental Research Letters*, 14(5), 054002. <https://doi.org/10.1088/1748-9326/ab13bf>.
- Lansu, E.M., van Heerwaarden, C.C., Stegehuis, A.I. and Teuling, A.J. (2020) Atmospheric aridity and apparent soil moisture drought in European forest during heatwaves. *Geophysical Research Letters*, 47, e2020GL087091. <https://doi.org/10.1029/2020GL087091>.
- Li, M., Wu, P. and Ma, Z. (2020) A comprehensive evaluation of soil moisture and soil temperature from third generation atmospheric and land reanalysis data sets. *International Journal of Climatology*, 40, 5744–5766. <https://doi.org/10.1002/joc.6549>.
- Lu, J., Tang, R., Tang, H. and Li, Z.-L. (2014) A new parameterization scheme for estimating surface energy fluxes with

- continuous surface temperature, air temperature, and surface net radiation measurements. *Water Resources Research*, 50, 1245–1259.
- Magnusson, L., Ferranti, L. and Vamborg, F. (2018) Forecasting the 2018 European heatwave. *ECMWF Newsletter*, 157, 4.
- McDonnell, J., Lambkin, K., Fealy, R., Hennessy, D., Shalloo, L. and Brophy, C. (2018) Verification and bias correction of ECMWF forecasts for Irish weather stations to evaluate their potential usefulness in grass growth modelling. *Meteorological Applications*, 25, 292–301.
- McEniry, J., Crosson, P., Finneran, E., McGee, M., Keady, T.W.J. and O’Kiely, P. (2013) How much grassland biomass is available in Ireland in excess of livestock requirements? *Irish Journal of Agricultural and Food Research*, 52, 67–80.
- McKee, T.B., Doesken, N.J. and Kleist, J. (1993) The relationship of drought frequency and duration to time scale. In: *Proceedings of the Eighth Conference on Applied Climatology, Anaheim, California, 17–22 January 1993*. Boston, MA: American Meteorological Society, pp. 179–184.
- Met Eireann Report. (2018) *A summer of heatwaves and droughts*. Available at: <https://www.met.ie/cms/assets/uploads/2018/09/summerfinal3.pdf> [Accessed November 2019].
- Miralles, D.G., Gentile, P., Seneviratne, S.I. and Teuling, A.J. (2019) Land-atmosphere feedbacks during droughts and heatwaves: state of the science and current challenges. *Annals of the New York Academy of Sciences*, 1436, 19–35. <https://doi.org/10.1111/nyas.13912>.
- Miralles, D.G., Teuling, A.J., van Heerwaarden, C.C. and de Arellano, J.-G. (2014) Mega-heatwave temperatures due to combined soil desiccation and atmospheric heat accumulation. *Nature Geoscience*, 7(5), 345–349.
- Monteith, J. (1981) Evaporation and surface temperature. *Quarterly Journal of the Royal Meteorological Society*, 107, 1–27.
- Moore, P. (2020) *Summer 2018*. Available at: <https://www.met.ie/cms/assets/uploads/2020/06/Summer2018.pdf> [Accessed February 2021].
- Muggeo, V.M.R. (2003) Estimating regression models with unknown break-points. *Statistics in Medicine*, 22(19), 3055–3071. <https://doi.org/10.1002/sim.1545>.
- Muggeo, V.M.R. (2021) Regression models with break-points/change-points estimation. An R “segmented” package version 1.3-3.
- Noone, S., Broderick, C., Duffy, C., Matthews, T., Wilby, R.L. and Murphy, C. (2017) A 250-year drought catalogue for the Island of Ireland (1765–2015). *International Journal of Climatology*, 37(S1), 239–254.
- Paulson, C.A. (1970) The mathematical representation of wind speed and temperature profiles in the unstable atmospheric surface layer. *Journal of Applied Meteorology and Climatology*, 9, 857–861.
- Peel, M.C., Finlayson, B.L. and McMahon, T.A. (2007) Updated world map of the Köppen–Geiger climate classification. *Hydrology and Earth System Sciences*, 11, 1633–1644.
- Rösner, B., Benedict, I., van Heerwaarden, C., Weerts, A., Hazeleger, W., Bissolli, P. and Trachte, K. (2019) The long heat wave and drought in Europe in 2018. *Bulletin of the American Meteorological Society*, 100(9), S222–S223.
- Schaaf, C. and Wang, Z. (2015) MCD43A4 MODIS/Terra+ Aqua BRDF/Albedo Nadir BRDF Adjusted Ref Daily L3 Global-500 m V006. NASA EOSDIS Land Processes DAAC. <https://doi.org/10.5067/MODIS/MCD43A4.006>
- Schuldts, B., Buras, A., Arend, M., Vitasse, Y., Beierkuhnlein, C., Damm, A., Gharun, M., Grams, T.E.E., Hauck, M., Hajek, P., Hartmann, H., Hiltbrunner, E., Hoch, G., Holloway-Phillips, M., Korner, C., Larysch, E., Lubbe, T., Nelson, D.B., Rammig, A., Rigling, A., Rose, L., Ruehr, N.K., Schumann, K., Weiser, F., Werner, C., Wohlgemuth, T., Zang, C.S. and Kahmen, A. (2020) A first assessment of the impact of the extreme 2018 summer drought on central European forests. *Basic and Applied Ecology*, 45, 86–103.
- Seneviratne, S.I., Corti, T., Davin, E.L., Hirschi, M., Jaeger, E.B., Lehner, I., Orlowsky, B. and Teuling, A.J. (2010) Investigating soil moisture–climate interactions in a changing climate: a review. *Earth Science Reviews*, 99, 125–161.
- Stap, L.B., van den Hurk, B.J.J.M., van Heerwaarden, C.C. and Neggers, R.A.J. (2014) Modeled contrast in the response of the surface energy balance to heatwaves for forest and grassland. *Journal of Hydrometeorology*, 15, 973–989.
- Streck, N.A. (2003) Stomatal response to water vapor pressure deficit: an unsolved issue. *Current Agricultural Science and Technology*, 9(4), 317–322.
- Teuling, A.J. (2018) A hot future for European droughts. *Nature Climate Change*, 8, 364–365.
- Teuling, A.J., Seneviratne, S.I., Stöckli, R., Reichstein, M., Moors, E., Ciais, P., Luysaert, S., van den Hurk, B., Ammann, C., Bernhofer, C., Dellwik, E., Gianelle, D., Gielen, B., Grunwald, T., Klumpp, K., Montagnani, L., Moureaux, C., Sottocornola, M. and Wohlfahrt, G. (2010) Contrasting response of European forest and grassland energy exchange to heatwaves. *Nature Geoscience*, 3(10), 722–727.
- van de Boer, A., Moene, A.F., Graf, A., Simmer, C. and Holtlag, A. A.M. (2014) Estimation of the refractive index structure parameter from single-level daytime routine weather data. *Applied Optics*, 53(26), 5944–5960.
- van Hateren, T.C., Chini, M., Matgen, P. and Teuling, A. (2021) Ambiguous agricultural drought: characterising soil moisture and vegetation droughts in Europe from earth observation. *Remote Sensing*, 13(10), 1990. <https://doi.org/10.3390/rs13101990>.
- van Heerwaarden, C.C. and Teuling, A.J. (2014) Disentangling the response of forest and grassland energy exchange to heatwaves under idealized land–atmosphere coupling. *Biogeosciences*, 11, 6159–6171.
- van Heerwaarden, C.C., Vila-Guerau de Arellano, J., Gounou, A., Guichard, F. and Couvreur, F. (2010) Understanding the daily cycle of evapotranspiration: a method to quantify the influence of forcings and feedbacks. *Journal of Hydrometeorology*, 11(6), 1405–1422.
- van Loon, A.F. (2015) Hydrological drought explained. *WIREs Water*, 2, 359–392.
- van Ulden, A.P. and Holtlag, A.A.M. (1985) Estimation of atmospheric boundary layer parameters for diffusion applications. *Journal of Applied Meteorology and Climatology*, 24, 1196–1207.
- Verger, A., Baret, F. and Weiss, M. (2014) Near real time vegetation monitoring at global scale. *IEEE Journal of Selected Topics in Applied Earth Observations and Remote Sensing*, 7, 3473–3481.
- Walsh, S. (2012) *A summary of climate averages for Ireland, 1981–2010*. Dublin: MET Eireann. Climatological Note No. 14. Available at: <https://www.met.ie/climate-ireland/SummaryClimAvgs.pdf>.

- Wan, Z., Hook, S. and Hulley, G. (2015) MOD11A1 MODIS/Terra Land Surface Temperature/Emissivity Daily L3 Global 1km SIN Grid V006. NASA EOSDIS Land Processes DAAC [Accessed on 29th January 2021] <https://doi.org/10.5067/MODIS/MOD11A1.006>
- Xiao, J., Zhuang, Q., Liang, E., Shao, X., McGuire, A.D., Moody, A., Kicklighter, D.W. and Melillo, J.M. (2009) Twentieth-century droughts and their impacts on terrestrial carbon cycling in China. *Earth Interactions*, 13, 1–31.
- Zaitchik, B.F., Macalady, A.K., Bonneau, L.R. and Smith, R.B. (2006) Europe's 2003 heat wave: a satellite view of impacts and land–atmosphere feedbacks. *International Journal of Climatology*, 26, 743–769.
- Zhang, L., Xiao, J., Li, J., Wang, K., Lei, L. and Guo, H. (2012) The 2010 spring drought reduced primary productivity in south-western China. *Environmental Research Letters*, 7(4), 1748–9326.
- Zscheischler, J., Westra, S., Hurk, B., Seneviratne, S.I., Ward, P.J., Pitman, A., Agha Kouchak, A., Bresch, D.N., Leonard, M.,

Wahl, T. and Zhang, X. (2018) Future climate risk from compound events. *Nature Climate Change*, 8(6), 469–477.

SUPPORTING INFORMATION

Additional supporting information can be found online in the Supporting Information section at the end of this article.

How to cite this article: Ishola, K. A., Mills, G., Fealy, R. M., & Fealy, R. (2023). A model framework to investigate the role of anomalous land surface processes in the amplification of summer drought across Ireland during 2018. *International Journal of Climatology*, 43(1), 480–498. <https://doi.org/10.1002/joc.7785>